CAAI Transactions on Intelligence Technology
ISSN 2468-2322 01/08 pp 1-9
Volume 2, Issue 4, December 2017

Magnetic Orientation System Based on Magnetometer, Accelerometer and Gyroscope

Zhiwei Chu Chilai Chen , Youjiang Liu, Yingxian Wang, and Xinhua Lin*

Zhiwei Chu, Chilai Chen, Youjiang Liu, Yingxian Wang, and Xinhua Lin are with the State Key Laboratory of Transducer Technology, Hefei Institute of Physical Science, Chinese Academy of Sciences, Hefei 230031, China. E-mail: xhlin@iim.ac.cn (Xinhua Lin).
Zhiwei Chu is with Department of Automation, School of Information Science and Technology, University of Science and Technology of China, Hefei 230026, China.
Zhiwei Chu, Chilai Chen, Youjiang Liu, Yingxian Wang, and Xinhua Lin are with the Key Laboratory of Biomimetic Sensing and Advanced Robot Technology of Anhui Province, Hefei Institute of Physical Science, Chinese Academy of Sciences, Hefei 230031, China.

*To whom correspondence should be addressed.

Manuscript received: 2017-09-09; accepted: 2017-11-20

Abstract: Magnetic orientation systems have widely been used by measuring earth magnetic field and provide a pervasive source of directional information. However, to obtain the high precision, orientation systems must be compensated prior to use for the various errors of magnetometers like the bias, misalignment and inconsistence in sensitivity, and the pitch and roll angles, especially in dynamic state. In this paper, magnetic orientation system mainly consisting of three single axis magnetometers, a tri-axis accelerometer and a tri-axis gyroscope was developed. An error-separation method was introduced to calibrate magnetometers. Data from magnetometers, accelerometer and gyroscope were fused based on Kalman filtering. In addition, accelerometer and gyroscope were also calibrated before data fusion, respectively. Experimental results showed the heading error of magnetic orientation system was about 0.1° in static state, and less than 3° in dynamic state, which proved the effectivity of the calibration methods and data fusion algorithm.

Key words: magnetic orientation; gyroscope; calibration; Kalman filtering

1 Introduction

The magnetic azimuth is the angle relative to the orientation of the earth magnetic field component in the horizontal plane, indicating the knowledge of the horizontal or vertical plane must be required to correct the measured magnetic value in the application of magnetic orientation systems. The tilt angles are commonly obtained by measuring the gravity vector at rest. In the previous report [1], it has been shown that the azimuth derived from the values of magnetometers and tilt contains and propagates the errors present in the attitude angles themselves. Thus, the orientation precision of magnetic orientation systems not only depends on the calibration validity of magnetometers, but also was closely related to the errors of tilt angles.

Usually, accelerometers are used to compensate for the azimuth by achieving attitude angles information [2-8]. In these references, the magnetic orientation systems have high precision partly because they are working in static state. However, when the magnetic orientation system works in dynamical state, the acceleration field obtained from the accelerometers contains kinematic acceleration besides gravitational acceleration. Thus, the real dynamic attitude of magnetic orientation systems can't be resolved from the output of accelerometers. As a result, just based on the data of magnetometers and accelerometers the azimuth error of magnetic orientation systems will be enlarged in the case of movement. Especially, when the kinematic acceleration disturbance is violent, the magnetic orientation systems will lose its functionality.

To deal with this problem, gyroscopes are introduced into magnetic orientation systems [10-12, 15]. These studies mainly focus on the sensor fusion algorithms and less analysis is applied to the calibration of sensors. However, the large measurement error in the output of sensors will lead to the large error of the data fusion results and poor convergence ability. Thus, at first magnetometer, accelerator and gyroscope in magnetic orientation system must be calibrated in order to obtain the actual real-time azimuth and attitude through the data fusion algorithm. Complementary filter (CF) algorithm is widely used in the field of unmanned aerial vehicles (UAV) and micro aerial vehicles (MAV). For the CF, a set of attitude angles are estimated in each measurement and they are multiplied with the corresponding gain factors. The eventual attitude angles are the sum of the parts. The more accurate estimations can be made by adjusting the gain factors. CF can be realized easily, but its accuracy is relatively low. It is only suitable for the low-dynamic application due to its slow response [16-18, 20]. The quaternion based extended Kalman filter (EKF) is appropriate for

non-linear plant models. Among the variants of the Kalman filtering framework, EKF is the most prominent one for its relatively high accuracy. However, in this algorithm the magnetic measurement is fused into roll and pitch, resulting in the larger error of yaw and the low precision in the pitch and roll angles once magnetic interference occurs [10, 18, 19, 21]. In addition, Jacobi matrix needs to be calculated in EKF, which will introduce the linearization error inevitably.

Based on the previous studies of the tri-axis magnetometer calibration with error-separation method [8], the tri-axis accelerometer calibration with multi-position method [5, 6] and the tri-axis gyroscope calibration through the method of three-position with six different angular velocities [9], a quaternion based Kalman filter (KF) is proposed in this paper to fuse the data from sensors and to estimate the orientation. In the measurement model, the state vector of quaternion is converted from the Euler angles which are resolved from the output of accelerometer and magnetometers instead of the accelerometer and magnetometers measurement vectors which are used in the traditional method of EKF [19]. So we can apply KF to the system without calculating Jacobi matrix since the process model and the measurement model are linear, which means no linearization error, lower cost of computation and less computational time. Better yet, when magnetic disturbances are present their influence is only limited to the heading angle. The achievement of the high-precise magnetic orientation system which can work well under various operation conditions demonstrated that the calibration and data fusion algorithm of multi-sensors are effective. And, the magnetic orientation system is suited to the practical application since it is composed of commercial-off-the-shelf components.

2 The Principle of Magnetic Orientation System without Gyroscope

The case body frame of magnetic orientation system is denoted as the b coordinate frame and has three orthogonal axes of x_b, y_b and z_b. We define that x_l, y_l and z_l are the axes of the local horizontal frame (l). The x_l is along the direction of horizontal projection of x_b, z_l is along the downward direction, and x_l, y_l and z_l obey the right-hand rule.

So, if θ denotes the pitch angle of the vehicle and φ denotes roll angle of the vehicle, the components of Earth magnetic field in the x_l and y_l direction can be calculated as follows:

$$\begin{aligned} h_x^l &= h_x^b \cos\theta + h_y^b \sin\theta \sin\varphi + h_z^b \sin\theta \cos\varphi \\ h_y^l &= h_y^b \cos\varphi - h_z^b \sin\varphi \end{aligned} \quad (1)$$

The magnetic heading ψ is obtained by the following formula:

$$\psi = \begin{cases} -\arctan(h_y^l / h_x^l), & (h_x^l > 0, h_y^l \le 0) \\ \pi/2, & (h_x^l = 0, h_y^l < 0) \\ \pi - \arctan(h_y^l / h_x^l), & (h_x^l < 0) \\ 3\pi/2, & (h_x^l = 0, h_y^l > 0) \\ 2\pi - \arctan(h_y^l / h_x^l), & (h_x^l > 0, h_y^l > 0) \end{cases} \quad (2)$$

where h_i^l (i=x, y or z) is the component of Earth magnetic field on the i axes in l frame; h_i^b is the component of Earth magnetic field on the i axes in b frame. According to the first order Taylor development of the azimuth computation [1], the uncertainty in azimuth becomes:

$$\psi + \Delta\psi = \arctan(\frac{-h_y^l}{h_x^l}) + \frac{\partial(\arctan(\frac{-h_y^l}{h_x^l}))}{\partial h_x^l}\Delta h_y^l + \frac{\partial(\arctan(\frac{-h_y^l}{h_x^l}))}{\partial h_y^l}\Delta h_x^l \quad (3)$$

Simplifying (3) and taking into account that:

$$H_e = H_h \begin{bmatrix} \cos\psi \\ -\sin\psi \\ \tan\delta \end{bmatrix} \quad (4)$$

where δ is the inclination of the magnetic vector and H_h the horizontal magnetic field. The error produced can be written as:

$$\Delta\psi = -\Delta\theta \cdot \tan\delta \cdot \cos\psi - \Delta\varphi \cdot \tan\delta \cdot \sin\psi \quad (5)$$

According to the above Eqs. (1), (2) and (5), in order to improve the precision of the heading angle ψ, we must not only increase the measurement precision of h_i^b as possible, but also take into account how to compensate the errors of pitch angle θ and roll angle φ.

3 Calibration of Sensors

The magnetic orientation system we developed comprises with three single axis magnetometers, a tri-axis accelerometer, and a tri-axis gyroscope. The calibration methods of sensors will be

introduced as follows.

3.1 Calibration of three single axis magnetometers

According to Eq. (2), the absolute magnitude of $h_i(i=x,y,z)$ is not necessary to compute the magnetic heading. In this paper, the error-separation method [8] is adopted to calibrate the magnetometers in consideration that it is convenient to evaluate the influence of different error sources and to get high precision of measurement. The output model of magnetometers can be expressed as follows:

$$\begin{bmatrix} h_x^m \\ h_y^m \\ h_z^m \end{bmatrix} = \begin{bmatrix} k_x^m & 0 & 0 \\ 0 & k_y^m & 0 \\ 0 & 0 & k_z^m \end{bmatrix} \begin{bmatrix} \cos\angle x_m x_b & \cos\angle x_m y_b & \cos\angle x_m z_b \\ \cos\angle y_m x_b & \cos\angle y_m y_b & \cos\angle y_m z_b \\ \cos\angle z_m x_b & \cos\angle z_m y_b & \cos\angle z_m z_b \end{bmatrix} \begin{bmatrix} h_x^b \\ h_y^b \\ h_z^b \end{bmatrix} + \begin{bmatrix} b_x^m \\ b_y^m \\ b_z^m \end{bmatrix} + \begin{bmatrix} n_x^m \\ n_y^m \\ n_z^m \end{bmatrix} \quad (6)$$

where $h_i^m(i=x,y,z)$ is the raw output of magnetometer, $k_i^m(i=x,y,z)$ is the sensitivity of the magnetometer in the direction of i_m, $\cos\angle A_m B_b(A,B=x,y,z)$ is the cosine of the angles between the relevant axes in the measurement frame and in the body frame, $b_i^m(i=x,y,z)$ is the bias originated from the offset and magnetic interference, $n_i^m(i=x,y,z)$ represents the noise of sensor and can be easily eliminated by averaging the measurements and thereafter, is ignored in this paper.

At the right side of Eq. (6), the first diagonal matrix accounts for the different sensitivities of the magnetometers, the second 3×3 matrix represents the output influence from non-orthogonality and misalignment of the three magnetometers, and the bias is embodied in the matrix about b.

With the three-axis non-magnetic rotation platform, the parameters in Eq. (6) can be obtained, so the errors from the sensitivity inconsistency, the non-orthogonality and misalignment and the combined biases can be eliminated independently. Now we get the output components of

earth magnetic field in the body frame as follows:

$$\begin{bmatrix} h_x^b \\ h_y^b \\ h_z^b \end{bmatrix} = \begin{bmatrix} \cos\angle x_m x_b & \cos\angle x_m y_b & \cos\angle x_m z_b \\ \cos\angle y_m x_b & \cos\angle y_m y_b & \cos\angle y_m z_b \\ \cos\angle z_m x_b & \cos\angle z_m y_b & \cos\angle z_m z_b \end{bmatrix}^{-1} \begin{bmatrix} k_x^m & 0 & 0 \\ 0 & k_y^m & 0 \\ 0 & 0 & k_z^m \end{bmatrix}^{-1} \begin{bmatrix} h_x^m - b_x^m \\ h_y^m - b_y^m \\ h_z^m - b_z^m \end{bmatrix} \tag{7}$$

Finally, the magnetic heading can be calculated by above Eqs. (1) and (2). After the calibration of magnetometers is accomplished, the relevant parameters are also acquired. The angles between the axes in the measurement frame and the body frame are shown in Table 1. The characteristic curves of magnetometers acquired with a linear least squares fit are shown in Fig. 1. According to the fitted curves, the parameters in the calibration matrix could be obtained. The result is shown as follows:

$$\begin{cases} k_x^m = 1751.15(LSB \cdot H_e^{-1}) \\ k_y^m = 1720.05(LSB \cdot H_e^{-1}) \\ k_z^m = 1717.16(LSB \cdot H_e^{-1}) \end{cases} \qquad \begin{cases} b_x^m = 61.93(LSB) \\ b_y^m = -114.52(LSB) \\ b_z^m = -183.77(LSB) \end{cases}$$

Now all the parameters to calibrate the magnetometers have been obtained. And if the true pitch angle and roll angle (as in static state) are known, we can determine orientation of the vehicle precisely with equations (1) and (2).

Table 1 Angles between the axes in the measurement frame and the body frame.

$\angle x_m x_b$	$\angle x_m y_b$	$\angle x_m z_b$
0.0640°	89.8353°	89.4179°
$\angle y_m x_b$	$\angle y_m y_b$	$\angle y_m z_b$
88.8302°	1.9147°	91.5156°
$\angle z_m x_b$	$\angle z_m y_b$	$\angle z_m z_b$
90.8175°	90.8175°	3.0661°

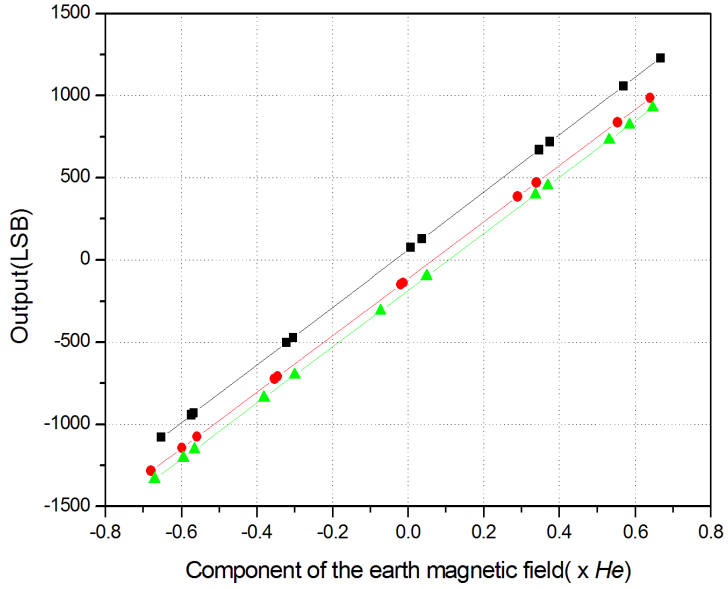

Fig. 1 Fitted curves between the outputs of magnetometers and the component of the earth magnetic field in the direction of the magnetic sensor axes (x_m axis: —, y_m axis: — and z_m axis: —) and the original outputs of magnetometers (x_m axis: ■, y_m axis: ● and z_m axis: ▲); He is equal to the magnitude of the earth magnetic field.

3.2 Calibration of tri-axis accelerometer

Unlike magnetometer, the accelerometer is immune to environmental impact because the gravity vector stays almost unchanged wherever it works. There are lots of methods to calibrate the tri-axis accelerometer. The so-called multiposition calibration is used mostly hitherto and has been proved to be effective [5, 6].

Table 2 Sign definition of the tri-axis accelerometer raw measurements.

Stationary position	Accelerometer (signed integer)		
	A_x^b	A_y^b	A_z^b
Z_b down	0	0	+1 (g)

Z_b	up	0	0	-1 (g)
Y_b	down	0	+1 (g)	0
Y_b	up	0	-1 (g)	0
X_b	down	-1 (g)	0	0
X_b	up	+1 (g)	0	0

In the six-position method, the sign definition of the accelerometer raw measurements is shown in Table 2. It's worth mentioning that to compute the tilt more effectively, A_x^b is defined along the direction of x_b and, A_y^b and A_z^b are in the opposite directions of y_b and z_b, respectively. The relationship between the normalized A_i^b (i=x, y or z) and the raw measurement A_i (i=x, y or z) of accelerometer can be expressed as the following equation.

$$\begin{bmatrix} A_x^b \\ A_y^b \\ A_z^b \end{bmatrix} = [A\_m]_{3\times3} \begin{bmatrix} 1/A\_S_x & 0 & 0 \\ 0 & 1/A\_S_y & 0 \\ 0 & 0 & 1/A\_S_z \end{bmatrix} \begin{bmatrix} A_x - A\_O_x \\ A_y - A\_O_y \\ A_z - A\_O_z \end{bmatrix} \quad (8)$$
$$= \begin{bmatrix} A_{11} & A_{12} & A_{13} \\ A_{21} & A_{22} & A_{23} \\ A_{31} & A_{32} & A_{33} \end{bmatrix} \begin{bmatrix} A_x \\ A_y \\ A_z \end{bmatrix} + \begin{bmatrix} A_{10} \\ A_{20} \\ A_{30} \end{bmatrix}$$

where $[A\_m]_{3\times3}$ is the 3×3 matrix representing the misalignment between the accelerometer sensing axes and the device body axes. A_S_i (i=x, y or z) is the sensitivity and A_O_i (i=x, y or z) is the offset.

Then, the pitch and roll angles of device can be calculated as the following:

$$Pitch(\theta) = \arctan\left(\frac{A_x^b}{\sqrt{(A_y^b)^2 + (A_z^b)^2}}\right) \quad (9)$$

$$Roll(\varphi) = \arctan\left(\frac{A_y^b}{A_z^b}\right) \quad (10)$$

According to the above formulas, the absolute magnitude of A_i^b (i=x, y or z) are not needed. Thus the normalized value A_i^b (i=x, y or z) can be obtained from any given raw measurements at arbitrary position as the following:

$$|A| = \sqrt{(A_x^b)^2 + (A_y^b)^2 + (A_z^b)^2} = 1 \quad (11)$$

According to the above equations (8-10), we need 12 parameters from A_{10} to A_{33} to calibrate the tri-axis accelerometer. By mounting the magnetic orientation system on the 3-D rotation platform which has a high-precision digital encoder, calibration can be operated at 6 stationary positions as shown in Table 2. We collect at least 100 sets of data at each position and take the averages. The 12 desired coefficients are extracted from the obtained data by the least square method as shown in Table 3.

Table 3 Coefficients of calibration for the tri-axis accelerometer.

A_{11}	A_{12}	A_{13}	A_{10}
-0.0001773	0.0000016	0.0000016	-0.0155254
A_{21}	A_{22}	A_{23}	A_{20}
0.0000037	-0.0001800	-0.0000007	0.0227611
A_{31}	A_{32}	A_{33}	A_{30}
0.0000036	-0.0000004	0.0001801	-0.0048272

3.3 Calibration of tri-axis gyroscope

Tri-axis gyroscope works by sensing angular velocity around the three sensitive axes. However, to ensure high precision, tri-axis gyroscope must be calibrated before use [9].

The output model of the tri-axis gyroscope can be expressed in a matrix form as follows:

$$\begin{bmatrix} G_x^b \\ G_y^b \\ G_z^b \end{bmatrix} = [G\_m]_{3\times3} \begin{bmatrix} 1/G\_S_x & 0 & 0 \\ 0 & 1/G\_S_x & 0 \\ 0 & 0 & 1/G\_S_x \end{bmatrix} \begin{bmatrix} G_x - G\_O_x \\ G_y - G\_O_y \\ G_z - G\_O_z \end{bmatrix} = \begin{bmatrix} k_{11} & k_{12} & k_{13} \\ k_{21} & k_{22} & k_{23} \\ k_{31} & k_{32} & k_{33} \end{bmatrix} \begin{bmatrix} G_x \\ G_y \\ G_z \end{bmatrix} + \begin{bmatrix} k_{10} \\ k_{20} \\ k_{30} \end{bmatrix} \quad (12)$$

Where G_x, G_y and G_z are the raw measurements of the X-axis, Y-axis, and Z-axis of the gyroscope respectively, G_x^b, G_y^b and G_z^b are the true angular velocities around the X-axis, Y-axis, and Z-axis of the body frame, the 3×3 matrix about $[G\_m]$ accounts for misalignment between the sensitive axis and the body axis , $G\_S_i(i=x,y,z)$ is the scale factor and G_O_i is the zero bias. The calibration process is described in detail in reference [9]. Here, the method of

three-position with six different angular velocities is adopted.

The 12 parameters about k can be calculated with least square method as follows:

$$K = \left[P^T \cdot P \right]^{-1} \cdot P^T \cdot Y \tag{13}$$

$$K = \begin{bmatrix} k_{11} & k_{21} & k_{31} \\ k_{12} & k_{22} & k_{32} \\ k_{13} & k_{23} & k_{33} \\ k_{10} & k_{20} & k_{30} \end{bmatrix} \tag{14}$$

$$P = \begin{bmatrix} G_1 & G_2 & \dots & G_{18} \end{bmatrix}^T \tag{15}$$

$$Y = \begin{bmatrix} y_1 & y_2 & \dots & y_{18} \end{bmatrix}^T \tag{16}$$

where $G_i (i = 1,2,...,18)$ is a 4×1 matrix $\begin{bmatrix} G_x & G_y & G_z & 1 \end{bmatrix}^T$, the elements are the values gotten from the calibration process and 1. $y_i (i = 1,2,...,18)$ is a 3×1 matrix consists of normalized output $\begin{bmatrix} G_x^b & G_y^b & G_z^b \end{bmatrix}^T$. As w_l, w_m and w_h are known [9], y_i is easy to determined.

After the processing of calibration, the matrix K is listed as follows:

$$K = \begin{bmatrix} -0.1243681 & -0.0012937 & -0.0033316 \\ 0.0003576 & 0.1237108 & 0.0009321 \\ 0.0003312 & -0.0001178 & -0.1243840 \\ -2.3843363 & 2.3942377 & -2.1203979 \end{bmatrix} \tag{17}$$

4 Data Fusion

In order to diminish the influence of non-gravitational acceleration, after the above calibrations, the data obtained from the sensors are further combined based on Kalman filtering with a state vector consisting of four elements (the quaternion components), a linear process model and a linear measurement model. The quaternion converted from Euler angles (computed with the Eqs. (2), (9) and (10)) is taken as the measurement for the Kalman filter to correct the predicted state obtained by processing the readings provided by the angular rate sensor (the tri-axis gyroscope). Using this method, all the output equations are linear, which simplifies the design of the filter, and

the nonlinear error from EKF can be eliminated.

4.1 Process model

In the prediction step, the angular velocity vector, measured by the tri-axis gyroscope, is used to compute the first estimation of the orientation in quaternion form. It is well known that the rigid body angular motion obeys a vector differential equation [10, 11] describing the rate of change of the orientation as quaternion derivative:

$$\frac{d}{dt}q = \Omega[\vec{w}]q \qquad (18)$$

where

$$\Omega[\vec{w}] = \frac{1}{2}\begin{bmatrix} [\vec{w}\times] & \vec{w} \\ -\vec{w}^T & 0 \end{bmatrix}. \qquad (19)$$

$$q = \begin{bmatrix} q_1 & q_2 & q_3 & q_4 \end{bmatrix}^T \qquad (20)$$

$\vec{w}(t) = [w_x \quad w_y \quad w_z]^T$ is the output of the tri-axis gyroscope after calibration. $\Omega[\vec{w}]$ is a 4×4 skew symmetric matrix and the operator

$$[\vec{w}\times] = \begin{bmatrix} 0 & w_z & -w_y \\ -w_z & 0 & w_x \\ w_y & -w_x & 0 \end{bmatrix} \qquad (21)$$

represents the standard vector cross-product [11].

In this paper, quaternion represents the notation from:

$$n = q_1 i + q_2 j + q_3 k + q_4 = \vec{n} + n_0 \qquad (22)$$

where q_1, q_2, q_3 and q_4 are real numbers and i, j, and k are unit vectors directed along the x, y, and z axis respectively. A quaternion is unit quaternion [12] if:

$$n_0 = \cos\theta \qquad \text{and} \qquad \left|\vec{n}\right| = \sin\theta \ .$$

The direct cosine matrix given in terms of the orientation quaternion can be expressed as the following matrix:

$$C_n^b(q)=\begin{bmatrix} q_1^2-q_2^2-q_3^2+q_4^2 & 2(q_1q_2+q_3q_4) & 2(q_1q_3-q_2q_4) \\ 2(q_1q_2-q_3q_4) & -q_1^2+q_2^2-q_3^2+q_4^2 & 2(q_2q_3+q_1q_4) \\ 2(q_1q_3+q_2q_4) & 2(q_2q_3-q_1q_4) & -q_1^2-q_2^2+q_3^2+q_4^2 \end{bmatrix} \quad (23)$$

Thus, we can establish the process model as the following:

$$q(k)=q(k-1)+\Omega[\vec{w}]q(k-1)\cdot dt+\zeta(k) \quad (24)$$

where k is the sampling number, dt is the sampling period, and

$$\zeta(k)=-\frac{dt}{2}\Xi(k)v_g(k)=-\frac{dt}{2}\begin{bmatrix} -q_4 & -q_3 & -q_2 \\ q_2 & -q_4 & -q_1 \\ -q_2 & q_1 & -q_4 \\ q_1 & q_2 & q_3 \end{bmatrix}v_g(k) \quad (25)$$

.

where $v_g(k)$ is the white Gaussian measurement noise affecting the gyroscope readings, with covariance matrix $\Sigma_g=\sigma_g^2\mathrm{I}_{3\times3}$. Finally, the process noise covariance matrix Q_k is expressed as:

$$Q_k=(-\frac{dt}{2})^2\Xi(k)\Sigma_g\Xi(k)^T \quad (26).$$

4.2 Measurement model

After calibration, the Euler angles can be computed with equations (2), (6) and (7) according to the output of the accelerometer and the magnetometers. The quaternion converted from the Euler angles is used in the measurement update step. The transformation formula is expressed in the reference [13]:

$$Z=\begin{bmatrix} q_1 \\ q_2 \\ q_3 \\ q_4 \end{bmatrix}=\begin{bmatrix} s\varphi c\theta c\psi-c\varphi s\theta s\psi \\ c\varphi s\theta c\psi+s\varphi c\theta s\psi \\ c\varphi c\theta s\psi-s\varphi s\theta c\psi \\ c\varphi c\theta c\psi+s\varphi s\theta s\psi \end{bmatrix} \quad (27)$$

where $c\phi=\cos(\phi/2)$, $s\phi=\sin(\phi/2)$, θ is pitch angle, φ is roll angle, and ψ is heading angle (computed with Eqs. (2), (6) and (7)) . The measurement model can be expressed as the following equation:

$$Z(k) = q(k) + \xi(k) \tag{28}$$

where $\xi(k)$ is the measurement noise which is approximated as a white Gaussian noise obtained from the propagation of the acceleration and magnetic field measurement noise [14]. The measurement noise covariance matrix is R_k.

4.3 Kalman filter

As a recursive estimator, the following formulas are used in computation:

$$\begin{aligned}
&\vec{x}_k^- = A\vec{x}_{k-1}^-, \\
&P_k^- = AP_{k-1}A^T + Q_k, \\
&K_k = P_k^- H^T (HP_k^- H^T + R_k)^{-1}, \\
&\vec{x}_k = \vec{x}_k^- + K_k(Z_k - H\vec{x}_k^-), \\
&P_k = (I - K_k H)P_k^-,
\end{aligned} \tag{29}$$

where $\vec{x}_k^-$ is the priori estimation of state vector, $\vec{x}_k$ is the posteriori estimation of state vector, A is the state matrix, H is the observation matrix, P is the error covariance matrix, I is the identity matrix, and K is the matrix of Kalman filter gain [11].

After each iteration, the magnetic orientation can be gotten from $\vec{x}_k$. As expressed in reference [13], the Euler angles can be computed from quaternion using the following formulas:

$$\begin{cases}
\psi = (180/\pi) \cdot atan2(2(q_4 \cdot q_3 + q_1 \cdot q_2), 1 - 2(q_2^2 + q_3^3)) \\
\theta = (180/\pi) \cdot arcsin(2(q_4 \cdot q_2 - q_1 \cdot q_3)) \\
\varphi = (180/\pi) \cdot atan2(2(q_4 \cdot q_1 + q_3 \cdot q_2), 1 - 2(q_2^2 + q_1^3))
\end{cases} \tag{30}$$

5 Experimental Results

For verification of the calibration methods and the proposed algorithm of data fusion, a 3-D non-magnetic platform that can rotate around three axes by manual operation was used. Before data fusion, the accuracy of error-separation calibration method in static state is shown in Fig. 2 where the horizontal coordinate axis stands for platform readings. We can see that with the magnitudes of both pitch and roll angles increasing, the heading errors exhibited an increasing

trend. But the maximum error in the heading was only about 0.4° even if the magnitudes of both pitch and roll angles increased up to 60°. And precision comparisons of different calibration methods are listed in Table 4. The ellipsoid fitting method and the traditional method are provided by [5] and [7]. These results demonstrated that the calibration method of error- separation was very effective and efficient.

Table 4 The heading accuracies of different calibration methods in different attitudes.

Different attitudes	Error-separation	Ellipsoid fitting [5]	Traditional method [7]
pitch =0° , roll =0°	0.2°	0.4°	0.8°
pitch =-30°, roll =-30°	0.3°	0.8°	1°
pitch =-60° , roll =60°	0.4°	1.2°	1.6°

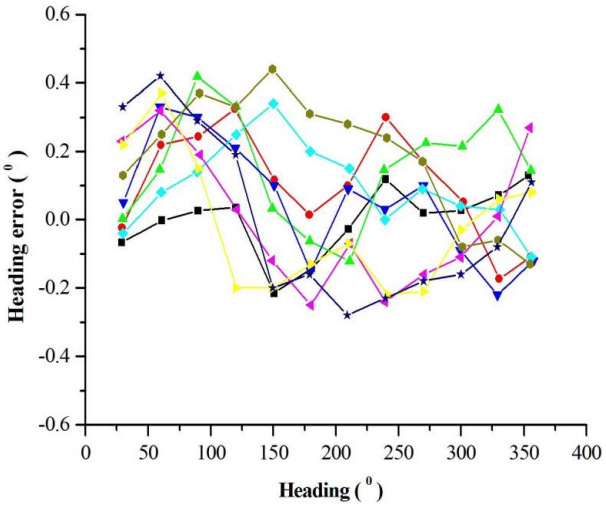

Fig. 2 Heading errors of magnetic orientation system with the different attitudes, (■) θ=0°, γ=0°; (▲) θ=30°, γ=30° and (▼) θ=30°, γ=-30°; (♦) θ=-30°, γ=30°; (◄)θ=-30°, γ=-30°; (●) θ=60°, γ=60°; (►) θ=60°, γ=-60°; (●)θ=-60°, γ=60° and (★) θ=-60°, γ=-60°.

After calibrating the sensors, two modes of experiments had been carried out to evaluate

accuracy of our magnetic orientation system. Mode 1 is the static state, and Mode 2 is the dynamic state. The results from the proposed Kalman filter (q-KF) are provided and for comparison, the corresponding results from EKF and CF are also shown.

In Mode 1, the magnetic orientation system was rigidly mounted on the 3-D non-magnetic platform and was kept static (remain level: true pitch and roll angles were equal 0°) when we were collecting data outputs. The results are shown in Fig. 3. The data called Measured (blue) were computed without data fusion only from the output of the tri-axis accelerometer and the magnetometers (as Eqs. (2), (9) and (10)), while the data called Estimated (green) were computed by the q-KF (as Eq. (30)). The black solid line called Reference represents the readings of the 3-D non-magnetic platform. We can see that with the Kalman filter algorithm proposed this paper, the magnetic orientation system is steadier (0.1°) than the one without data fusion (0.4°). And the errors of yaw, pitch, and roll angles computed by the data fusion in our magnetic orientation system are very small as about 0.1°.

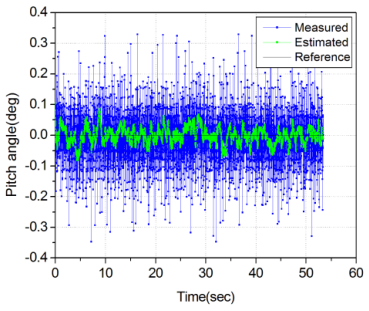

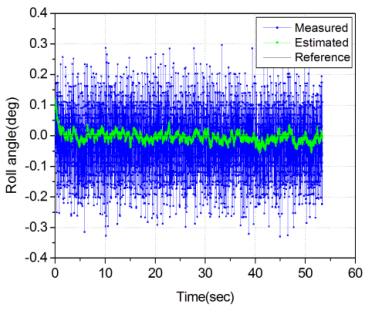

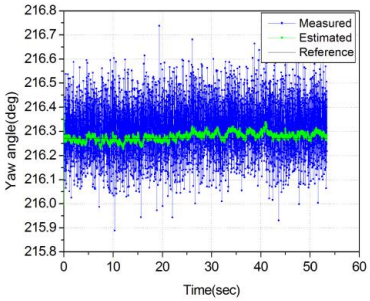

Fig. 3 Test in Mode 1: Outputs of pitch, roll and yaw angles in static state.

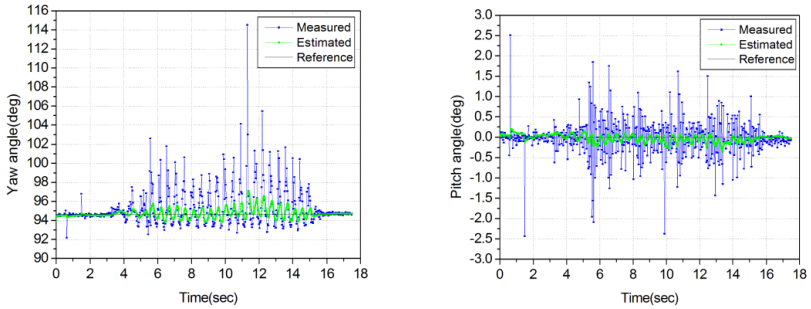

Fig. 4 Test in Mode 2 (a): Outputs of yaw and pitch angles in dynamic state when roll angle was dynamically changed.

In Mode 2, the magnetic orientation system was mounted on the 3-D non-magnetic platform, then we carried out two kinds of operation conditions (Mode 2 (a) and Mode 2 (b)). In Mode 2 (a), the roll angle was dynamically changed by manual operation when the pitch angle was kept at $0°$. From Fig. 4, it can be seen that after calibration and data fusion based on q-KF (Estimated), the maximum error of yaw angle was about $2.8°$ and the maximum error of pitch angle was about $0.3°$. But, without the data fusion (Measured) the maximum error of yaw angle was more than $10°$ and the maximum error of pitch angle was about $2.5°$. In Mode 2 (b), when the roll angle was kept at $0°$, the pitch angle was dynamically changed by manual operation. As shown in Fig. 5, with the q-KF the maximum errors of yaw and roll angles decreased from about $6.5°$ (Measured)

to about 2.5° (Estimated) and from about 2.5° (Measured) to about 1.8° (Estimated) in Mode 2 (b), respectively. The above results demonstrate that the heading and attitude precision were improved significantly with our calibration methods and data fusion algorithm based on Kalman filter. It's worth mentioning that since roll angle (Mode 2 (a)) and pitch angle (Mode 2 (b)) of the 3-D non-magnetic platform was changed by manual operation , their real angle values were unobservable during changing with time. Thus, the data of roll angles (Mode 2 (a)) and pitch angles (Mode 2 (b)) are not shown in this paper.

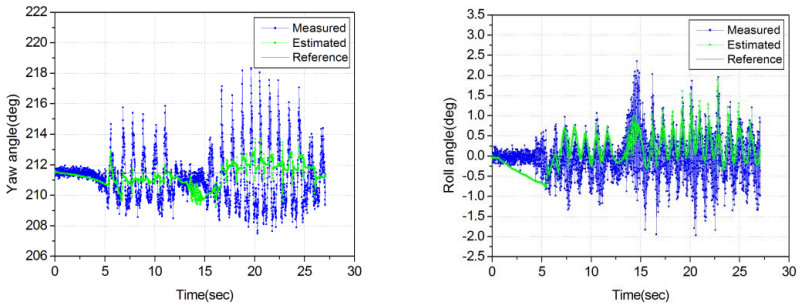

Fig. 5 Test in Mode 2 (b): Outputs of yaw and roll angles in dynamic state when pitch angle was dynamically changed.

Obviously, in the dynamic circumstance the magnetic orientation system without gyroscope and data fusion is useless and the errors, especially the error of yaw angle, are large. After this magnetic orientation system was applied with our calibration methods and data fusion algorithm, the error of yaw angle was less than 3° and the attitude (pitch and roll) errors were less than 2°. At last, the precision comparisons between different data fusion algorithms are shown in Table 5. The above experimental results show that our magnetic orientation system has the good performance and practicability even in dynamic work conditions.

Table 5 The heading accuracies of different data fusion methods in static and dynamic state.

Max error	Proposed Kalman filter (q-KF)	EKF[10,21]	CF[16,18,20]
Static	0.1°	0.2°	0.8°

Pitch dynamic	2.5°	3.2°	3.8°
Roll dynamic	2.8°	3.6°	3.9°

6 Conclusions

In this paper, the magnetic orientation system was developed with three magnetometers, a tri-axis accelerometer and a tri-axis gyroscope. Magnetometer and accelerometer were calibrated with the error-separation method and six-position method, respectively. And, the method of three-position with six different angular velocities was adopted for calibrating gyroscope. Finally, in order to keep the functionality of the magnetic orientation system in dynamic state, a data fusion algorithm base on linear Kalman filter (q-KF) was developed. The experimental results show that the accuracy of the heading and attitude was improved significantly both in static and dynamic states after the improved data fusion. The maximum error of yaw angle was about 0.1° in static state and 2.8° in dynamic state. And the maximum error of attitude (pitch/roll angle) was about 0.1° in static state and 1.8° in dynamic state. The achievement of magnetic orientation system with high precision demonstrated that the methods of calibration and the data fusion algorithm were effective and practical. It is worth mentioning that in terms of the estimation accuracy, due to the various dynamic conditions this paper does not claim that the parameters of Kalman filter are effective and suitable in any dynamic condition. In other words, the kinematic condition must be considered in term of the severity of the external accelerations in order to improve the estimation performance by adjusting the parameters of Kalman filter. Thus, a future research direction will be focused on an adaptive algorithm for learning the parameters in real time to further improve the adaptability of magnetic orientation systems.

Acknowledgment

The research is supported by National Natural Science Foundation of China (Project number: U1732152).

References

[1] Q. Ladetto, J. V. Seeters, S. Sokolowski S, Z. Sagan, and B. Merminod, Digital Magnetic Compass and Gyroscope for Dismounted Soldier Position & Navigation, in *Proceedings of NATO-RTO Meetings*, Istanbul, Turkey. 2002.

[2] M. Sipos, J. Rohac, and P. Novacek, Improvement of electronic compass accuracy based on magnetometer and accelerometer calibration, *Acta Phys. Polonica A*, vol. 121, no. 4, pp. 945–949, 2012.

[3] J. Včelák, P. Ripka, J. Kubík, A. Platil, and P. Kašpar, AMR navigation systems and methods of their calibration, *Sensors and Actuators A: Physical*, vol. 123-124, pp. 122-128, 2005.

[4] V. Renaudin, M. H. Afzal, and L. Gérard, Complete Triaxis Magnetometer Calibration in the Magnetic Domain, *Journal of Sensors*, vol. 2010, pp. 23-59, 2010.

[5] J. Fang, H. Sun H, J. Cao, X. Zhang, and Y. Tao , A Novel Calibration Method of Magnetic Compass Based on Ellipsoid Fitting, *IEEE Transactions on Instrumentation & Measurement*, vol. 60, no. 6, pp. 2053-2061, 2011.

[6] Z. F. Syed, P. Aggarwal, C. Goodall, X. Niu, and E. El-Sheimy, A new multi-position calibration method for MEMS inertial navigation systems, *Meas. Sci. Technol.*, vol. 18, pp. 1897–1907, 2007.

[7] J. Yun, J. Ko, J. Lee, and J. M. Lee, An inexpensive and accurate absolute position sensor for driving assistance, *IEEE Trans. Instrum. Meas.*,vol. 57, no. 4, pp. 864‑873, 2008.

[8] Z. Chu, X. Lin, K. Gao, and C. L. Chen, Error-separation method for the calibration of magnetic compass, *Sensors & Actuators A Physical*, vol. 250, pp. 195-201, 2016.

[9] X. D. Peng, Y. Chen, J. Y. Li, G. Q. Yan, and T. M. Zhang, Study on calibration method of MEMS 3-axis digital gyroscope, *Transducer & Microsystem Technologies*, vol. 32, no. 6, pp. 63-68, 2013.

[10] S. M. Sabatini, Quaternion-based extended Kalman filter for determining orientation by

inertial and magnetic sensing, *IEEE Transactions on Biomedical Engineering*,, vol. 53, no. 7, pp. 1346-1356, 2006.

[11] R. G. Valenti, I. Dryanovski, and J. Xiao, A Linear Kalman Filter for MARG Orientation Estimation Using the Algebraic Quaternion Algorithm, *IEEE Transactions on Instrumentation & Measurement*, vol. 65, no. 2, pp. 467-481, 2016.

[12] J. L. Marins, X. Yun, E. R. Bachmann, R.B. McGhee, and M.J. Zyda, An extended Kalman filter for quaternion-based orientation estimation using MARG sensors, in *Proceedings of 2001 IEEE/RSJ International Conference on Intelligent Robots and Systems*, 2001, vol. 4, pp. 2003-2011.

[13] M. D. Shuster, Survey of attitude representations, *Journal of the Astronautical Sciences*, vol. 41, no. 4, pp. 439-517, 1993.

[14] J. K. Lee, E. J. Park, and S. N. Robinovitch, Estimation of Attitude and External Acceleration Using Inertial Sensor Measurement During Various Dynamic Conditions, *IEEE Transactions on Instrumentation & Measurement*, vol. 61, no. 8, pp. 2262-2273, 2012.

[15] Y. H. Huang, Y. Rizal, and M. T. Ho, Development of attitude and heading reference systems, in *2015 International Automatic Control Conference(CACS)*, 2015, pp. 13-18.

[16] T. Gao, C. Shen, Z. Gong, J. Rao, and J. Luo, An Adaptive Filter for a Small Attitude and Heading Reference System Using Low Cost Sensors, *Advances in Computer, Communication, Control and Automation*, pp. 131-139, 2012.

[17] M. T. Leccadito, T. Bakker, R. Niu, and R. H. Klenke, *A Kalman Filter Based Attitude Heading Reference System Using a Low Cost Inertial Measurement Unit*. Virginia Commonwealth University, 2013.

[18] M. Nowicki, J. Wietrzykowski, and P. Skrzypczynski, Simplicity or flexibility? Complementary Filter vs. EKF for orientation estimation on mobile devices, in *2015 IEEE 2nd International Conference on Cybernetics (CYBCONF)*, 2015, pp. 166-171.

[19] R. G. Valenti, I. Dryanovski, and J. Xiao, A Linear Kalman Filter for MARG Orientation Estimation Using the Algebraic Quaternion Algorithm, *IEEE Transactions on Instrumentation & Measurement*, vol. 65, no. 2, pp. 467-481, 2016.

[20] Y. Naidoo, R. Stopforth, and G. Bright, Quad-rotor unmanned aerial vehicle helicopter

modelling & control, *International Journal of Advanced Robotic Systems*, vol. 8, pp. 139-149, 2011.

[21] R. Munguia and A. Grau, Attitude and Heading System based on EKF total state configuration, in *IEEE International Symposium on Industrial Electronics*, 2011, pp. 2147-2152.

Zhiwei Chu is currently a MS candidate at Institute of Intelligent Machines, Hefei Institute of Physical Sciences, Chinese Academy of Sciences and Department of Automation, School of Information Science and Technology, University of Science and Technology of China. His research interests include sensors, electronics, signal processing for low-cost precise navigation systems. TEL:18256013177.

Chilai Chen received the PhD degree in precision machinery and precision instruments at University of Science and Technology of China in 2011. At present, he is an associate researcher at Institute of Intelligent Machines, Hefei Institute of Physical Sciences, Chinese Academy of Sciences, China. His major interests are devices and instruments for monitoring environment.

Youjiang Liu received the PhD degree in control science and engineering at University of Science and Technology of China in 2015. Now, he is an assistant researcher at Institute of Intelligent Machines, Hefei Institute of Physical Sciences, Chinese Academy of Sciences, China. His main research interests are signal and information processing and weak signal detection.

Yingxian Wang is an associate researcher at Institute of Intelligent Machines, Hefei Institute of Physical Sciences, Chinese Academy of Sciences, China. Her main research interests are MEMs sensors preparation and application.

Xinhua Lin received the PhD degree in material science and engineering at Shanghai Institute Ceramics, Chinese Academy of Sciences, China in 2003. Now, he is an associate researcher at Institute of Intelligent Machines, Hefei Institute of Physical Sciences, Chinese Academy of Sciences, China. His main research interests are magnetic sensors and magnetic measurements.